



OPEN

Quantum-criticality-induced strong Kerr nonlinearities in optomechanical systems

SUBJECT AREAS:

NANOSCIENCE AND TECHNOLOGY

QUANTUM OPTICS

Received
22 August 2013Accepted
27 September 2013Published
15 October 2013

Correspondence and requests for materials should be addressed to

X.-Y.L. (xinyoulu@riken.jp) or F.N. (fnori@riken.jp)

¹CEMS, RIKEN, Saitama, 351-0198, Japan, ²Wuhan National Laboratory for Optoelectronics and School of Physics, Huazhong University of Science and Technology, Wuhan 430074, People's Republic of China, ³Department of Physics, National Cheng Kung University, Tainan 70101, Taiwan, ⁴Physics Department, The University of Michigan, Ann Arbor, Michigan 48109-1040, USA, ⁵Department of Physics, Korea University, Seoul 136-713, Republic of Korea.

We investigate a hybrid electro-optomechanical system that allows us to realize controllable strong Kerr nonlinearities even in the weak-coupling regime. We show that when the controllable electromechanical subsystem is close to its quantum critical point, strong photon-photon interactions can be generated by adjusting the intensity (or frequency) of the microwave driving field. Nonlinear optical phenomena, such as the appearance of the photon blockade and the generation of nonclassical states (e.g., Schrödinger cat states), are demonstrated in the weak-coupling regime, making the observation of strong Kerr nonlinearities feasible with currently available optomechanical technology.

Strong optical nonlinearity gives rise to many important quantum effects, such as photon blockade^{1–3}, quantum squeezing⁴, quantum nondemolition measurements^{5,6}, optical switching with single photon⁷ and so on^{8–10}. These nonlinear optical effects have been demonstrated in cavity QED systems, where the quantum coherence in the atom^{1–3} (or artificial atom^{11–17}) generates strong effective photon nonlinearities.

Recently, cavity optomechanics has become a rapidly developing research field exploring nonlinear coupling via radiation pressure between the electromagnetic and mechanical systems^{18–20}. It has been shown *theoretically* that strong optical nonlinear effects (and relevant applications, such as generating nonclassical state, photon blockade, multiple sidebands, photon-phonon transistors, and optomechanical photon measurement) can be realized in single-mode^{21–33} or two-mode optomechanical systems (OMSs)^{34,35}. These phenomena are mainly demonstrated in the single-photon strong-coupling regime, where the optomechanical coupling strength at the single-photon level g_a exceeds the cavity decay rate κ_a ($g_a > \kappa_a$). However, in most experiments to date^{36–38}, g_a is much smaller than κ_a ($g_a/\kappa_a \sim 10^{-3}$). Only a few new-type optomechanical setups, using ultracold atoms in optical resonators ($g_a/\kappa_a \sim 10^{-1}$)³⁹ or optomechanical crystals ($g_a/\kappa_a \sim 10^{-2}$)⁴⁰, can one begin to approach the single-photon strong-coupling regime. On the other hand, a strong optical driving field may effectively enhance the optomechanical coupling by a factor \sqrt{n} , where n is the mean photon number in the cavity^{41–43}. But this enhancement comes at the cost of losing the nonlinearity of the interactions. Specifically, under the condition of strong optical driving, the linearized coupling strength between the optical and mechanical modes is largely enhanced, which makes the intrinsic nonlinear optomechanical coupling smaller and negligible.

Given the above, it is highly desirable to find a new method for obtaining strong Kerr nonlinearities in OMSs in the *weak-coupling regime*, namely the optomechanical coupling strength is much smaller than the optical cavity decay rate ($g_a \ll \kappa_a$). In this paper, we investigate the Kerr nonlinear effects of the optical field in a hybrid electro-optomechanical system containing a mechanical oscillator coupled to both an optical cavity and a microwave LC resonator (see Fig. 1)^{44–47}. We find that the electromechanical subsystem (the mechanical oscillator plus the microwave resonator) displays a quantum criticality. One can drive the electromechanical subsystem close to the quantum critical regime by applying a microwave field with properly chosen frequency and intensity to the microwave resonator. Then the quantum criticality can induce a strong Kerr nonlinearity in the optical cavity, even if the optomechanical systems (the optical cavity and mechanical oscillator) is in the weak-coupling regime. This strong Kerr nonlinearity can be demonstrated by the existences of photon blockade and nonclassical states (e.g., Schrödinger cat states) of the cavity field when the electromechanical subsystem approaches the quantum critical point. Furthermore, the strong Kerr nonlinearity can also be controlled easily by tuning the intensity (or frequency) of the microwave driving field. This provides a promising route for experimentally observing strong Kerr nonlinearities in OMSs in the weak-coupling regime.

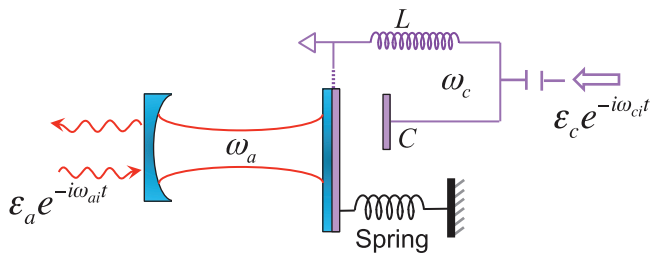


Figure 1 | Schematic diagram of the hybrid electro-optomechanical system. A mechanical oscillator couples to both an optical cavity and a microwave LC resonator.

Results

Hybrid electro-optomechanical system. In the hybrid electro-optomechanical system of Fig. 1, the mechanical oscillator is parametrically coupled to both the optical cavity and the microwave resonator. The microwave resonator is driven by a strong field with amplitude ε_c and frequency ω_{ci} , where ε_c is related to the input microwave power P and microwave decay rate κ_c by $|\varepsilon_c| = \sqrt{2P\kappa_c/\hbar\omega_{ci}}$. In a frame rotating with frequency ω_{ci} , the Hamiltonian for this hybrid systems reads⁴⁸

$$\hat{H}_{\text{OMS}}/\hbar = \delta_c \hat{c}^\dagger \hat{c} + \omega_a \hat{a}^\dagger \hat{a} + \omega_b \hat{b}^\dagger \hat{b} + g_a \hat{a}^\dagger \hat{a} (\hat{b}^\dagger + \hat{b}) + g_c \hat{c}^\dagger \hat{c} (\hat{b}^\dagger + \hat{b}) + i\varepsilon_c (\hat{c}^\dagger - \hat{c}), \quad (1)$$

where the detuning $\delta_c = \omega_c - \omega_{ci}$ and the microwave frequency $\omega_c = 1/\sqrt{LC}$, g_a (g_c) denotes the optomechanical (electromechanical) coupling strength at the single-photon level, and \hat{a} (\hat{b} or \hat{c}) is the annihilation operator of the optical cavity (the mechanical oscillator or the microwave resonator). Under a strong microwave driving field, following the standard linearization procedure^{49–52} (shifting \hat{c} and \hat{b} with their steady-state mean values α and β , i.e., $\hat{c} \rightarrow \hat{c} + \alpha$, $\hat{b} \rightarrow \hat{b} + \beta$), the Hamiltonian can be transformed into

$$\hat{H}'_{\text{OMS}}/\hbar = \Delta_c \hat{c}^\dagger \hat{c} + \tilde{\omega}_a \hat{a}^\dagger \hat{a} + \omega_b \hat{b}^\dagger \hat{b} + g_a \hat{a}^\dagger \hat{a} (\hat{b}^\dagger + \hat{b}) - G (\hat{c}^\dagger + \hat{c}) (\hat{b}^\dagger + \hat{b}), \quad (2)$$

where G is the linearized electromechanical coupling strength; Δ_c and $\tilde{\omega}_a$ are, respectively, the effective microwave detuning and optical frequency including the radiation-pressure-induced optical resonance shift. Their explicit expressions are given by

$$G = g_c \sqrt{\frac{2P\kappa_c}{\hbar(\omega_c - \delta_c)(\kappa_c^2 + \Delta_c^2)}}, \quad (3a)$$

$$\Delta_c = \delta_c - \frac{4g_c^2 P \kappa_c}{\hbar \omega_b (\omega_c - \delta_c)(\kappa_c^2 + \Delta_c^2)}, \quad (3b)$$

$$\hat{\omega}_a = \omega_a - \frac{4g_a g_c P \kappa_c}{\hbar \omega_b (\omega_c - \delta_c)(\kappa_c^2 + \Delta_c^2)}, \quad (3c)$$

Notice that G and Δ_c can be easily controlled by tuning the power and frequency of the microwave driving field.

Quantum critical property of the electromechanical subsystem. The quantum criticality in the electromechanical subsystem can be shown by diagonalizing the electromechanical subsystem via a Bogoliubov transformation $\hat{R} = M \hat{B}$. Here, the canonical operators are $\hat{R}^T = (\hat{c}, \hat{c}^\dagger, \hat{b}, \hat{b}^\dagger)$ and $\hat{B}^T = (\hat{B}_-, \hat{B}_+^\dagger, \hat{B}_+, \hat{B}_+^\dagger)$, and M is the transformation matrix given by

$$M = \begin{pmatrix} \frac{1}{2} \frac{\cos\theta}{\sqrt{\Delta_c \omega_-}} (\Delta_c + \omega_-) & \frac{1}{2} \frac{\cos\theta}{\sqrt{\Delta_c \omega_-}} (\Delta_c - \omega_-) \\ \frac{1}{2} \frac{\cos\theta}{\sqrt{\Delta_c \omega_-}} (\Delta_c - \omega_-) & \frac{1}{2} \frac{\cos\theta}{\sqrt{\Delta_c \omega_-}} (\Delta_c + \omega_-) \\ -\frac{1}{2} \frac{\sin\theta}{\sqrt{\omega_b \omega_-}} (\omega_b + \omega_-) & -\frac{1}{2} \frac{\sin\theta}{\sqrt{\omega_b \omega_-}} (\omega_b - \omega_-) \\ -\frac{1}{2} \frac{\sin\theta}{\sqrt{\omega_b \omega_-}} (\omega_b - \omega_-) & -\frac{1}{2} \frac{\sin\theta}{\sqrt{\omega_b \omega_-}} (\omega_b + \omega_-) \\ \frac{1}{2} \frac{\sin\theta}{\sqrt{\Delta_c \omega_+}} (\Delta_c + \omega_+) & \frac{1}{2} \frac{\sin\theta}{\sqrt{\Delta_c \omega_+}} (\Delta_c - \omega_+) \\ \frac{1}{2} \frac{\sin\theta}{\sqrt{\Delta_c \omega_+}} (\Delta_c - \omega_+) & \frac{1}{2} \frac{\sin\theta}{\sqrt{\Delta_c \omega_+}} (\Delta_c + \omega_+) \\ \frac{1}{2} \frac{\cos\theta}{\sqrt{\omega_b \omega_+}} (\omega_b + \omega_+) & \frac{1}{2} \frac{\cos\theta}{\sqrt{\omega_b \omega_+}} (\omega_b - \omega_+) \\ \frac{1}{2} \frac{\cos\theta}{\sqrt{\omega_b \omega_+}} (\omega_b - \omega_+) & \frac{1}{2} \frac{\cos\theta}{\sqrt{\omega_b \omega_+}} (\omega_b + \omega_+) \end{pmatrix},$$

where the angle θ is defined by

$$\tan 2\theta = \frac{4G_c \sqrt{\Delta_c \omega_b}}{\Delta_c^2 - \omega_b^2}.$$

Then, the Hamiltonian \hat{H}'_{OMS} becomes

$$\hat{H}'_{\text{OMS}}/\hbar = \omega_- \hat{B}_-^\dagger \hat{B}_- + \omega_+ \hat{B}_+^\dagger \hat{B}_+ + \tilde{\omega}_a \hat{a}^\dagger \hat{a} + g_- \hat{a}^\dagger \hat{a} (\hat{B}_-^\dagger + \hat{B}_-) + g_+ \hat{a}^\dagger \hat{a} (\hat{B}_+^\dagger + \hat{B}_+), \quad (4)$$

where ω_\pm are the normal mode frequencies of the electromechanical subsystem,

$$\omega_\pm^2 = \frac{1}{2} \left(\Delta_c^2 + \omega_b^2 \pm \sqrt{(\omega_b^2 - \Delta_c^2)^2 + 16G^2 \Delta_c \omega_b} \right), \quad (5)$$

and

$$g_\pm = \pm g_a \sqrt{\omega_b (1 \pm \cos 2\theta) / 2\omega_\pm}$$

are the effective coupling strengths between the optical photon and the normal modes. Equation (5) shows that ω_-^2 becomes zero (negative) when

$$G = G_{cp} = \sqrt{\Delta_c \omega_b} / 2 \quad (G > G_{cp}),$$

as shown in Fig. 2(a). This corresponds to a critical property⁵³, namely, the normal mode ω_- will change from a standard harmonic oscillator ($G < G_{cp}$) to a free particle, and further becomes dynamically unstable ($G > G_{cp}$) as G crosses its critical value G_{cp} .

The above critical property can become more transparent with the following canonical relationships:

$$\begin{aligned} \hat{b} &= \frac{1}{\sqrt{2}} (x_b + ip_b), & \hat{b}^\dagger &= \frac{1}{\sqrt{2}} (x_b - ip_b), \\ \hat{c} &= \frac{1}{\sqrt{2}} (x_c + ip_c), & \hat{c}^\dagger &= \frac{1}{\sqrt{2}} (x_c - ip_c). \end{aligned}$$

Here x_b, x_c are the dimensionless displacements of the mechanical and microwave resonators from their stable points, and p_b, p_c are the corresponding dimensionless momentums. The Hamiltonian of the electromechanical system can then be written in terms of the usual canonical $x-p$ variables, $H_{e-m} = H_0 + H_{\text{int}}$ with

$$H_0/\hbar = \frac{\Delta_c}{2} (p_c^2 + x_c^2) + \frac{\omega_b}{2} (p_b^2 + x_b^2), \quad (6a)$$

$$H_{\text{int}}/\hbar = -2Gx_c x_b, \quad (6b)$$

denoting the free Hamiltonian of the microwave and the mechanical resonators, and the coupling between them. The potential of the free

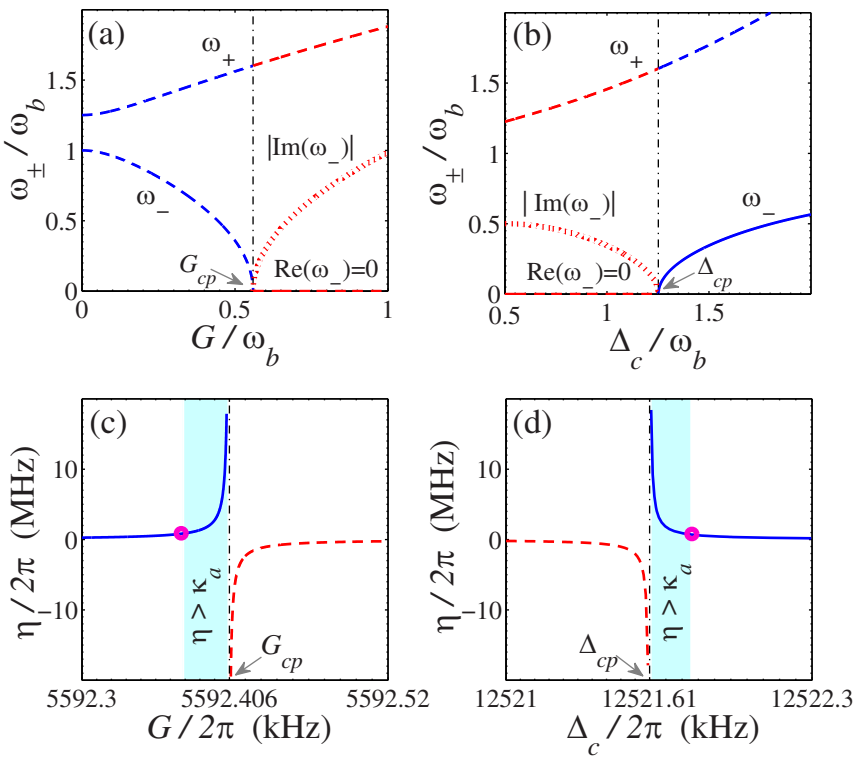


Figure 2 | Quantum criticality of the electromechanical subsystem and strong Kerr nonlinearity of the optical field. (a,b) Quantum criticality of the electromechanical subsystem, characterized by the normal-mode frequency ω_{\pm}/ω_b . As one can see, the normal-mode ω_+ continuously passes through the critical point. The quantum criticality is manifested with the normal-mode ω_- , which becomes purely imaginary after the critical point $G/\omega_b > 0.5$ and $\Delta_c/\omega_b < 1.25$ (c,d) Strong Kerr-nonlinearity given by the photon-photon interaction strength η in the optical cavity, as a function of the adjustable parameters G and Δ_c controlled by the microwave driving field. The pink circles and shaded area in (c,d) correspond, respectively, to the regimes $\eta = \kappa_a$ and $\eta > \kappa_a$. The black dot-dashed vertical lines indicate the quantum critical points G_{cp} and Δ_{cp} . Other system parameters are taken as: $\omega_b/2\pi = 10$ MHz, $g_a/\omega_b = g_c/\omega_b = 10^{-3}$, $\kappa_a/\omega_b = 0.1$, $\kappa_c/\omega_b = 0.125$, $\Delta_c/\omega_b = 1.251$ (a,c), and $G/\omega_b = 0.5595$ (b,d).

Hamiltonian (6a) can be further expressed as

$$\frac{\Delta_c}{2} x_c^2 + \frac{\omega_b}{2} x_b^2 = \frac{1}{2} \left(\sqrt{\Delta_c} x_c - \sqrt{\omega_b} x_b \right)^2 + \sqrt{\Delta_c \omega_b} x_c x_b. \quad (7)$$

It shows that the intrinsic potential of the electro and mechanical resonators is characterized by $\sqrt{\Delta_c \omega_b}$. Comparing Eq. (7) with the coupling Hamiltonian (6b), one can see that there is an interplay between the intrinsic potential and the coupling interaction between them. This interplay leads to the above critical property. In other words, when G approaches (or exceeds) $\sqrt{\Delta_c \omega_b}/2$, the normal mode ω_- is dragged out from its effective potential, and becomes increasingly flat (or inverted) [see the Fig. 3].

Quantum-criticality-induced strong Kerr nonlinearities. As one can see, the last two terms in the Hamiltonian (4) show that optical photons can interact with each other through the exchange of the normal modes \hat{B}_{\pm} , very similar to electrons interacting with each other through the exchange of photons in the QED Hamiltonian. In particular, when the electromechanical subsystem approaches its quantum critical point, the optical cavity shows a strong effective Kerr nonlinearity. This quantum-criticality-induced strong Kerr nonlinearity becomes clear after taking a displacement transformation, $\hat{H}'_{\text{OMS}} = \hat{V}^\dagger \hat{H}_{\text{OMS}} \hat{V}$, where $\hat{V} = \exp(-\hat{P} a^\dagger \hat{a})$ is a similarity transformation and $\hat{P} = \zeta_- \hat{P}_- + \zeta_+ \hat{P}_+$ with $\hat{P}_j = \hat{B}_j^\dagger - \hat{B}_j$ ($j = \pm$), $\zeta_{\pm} = g_{\pm}/\omega_{\pm}$.

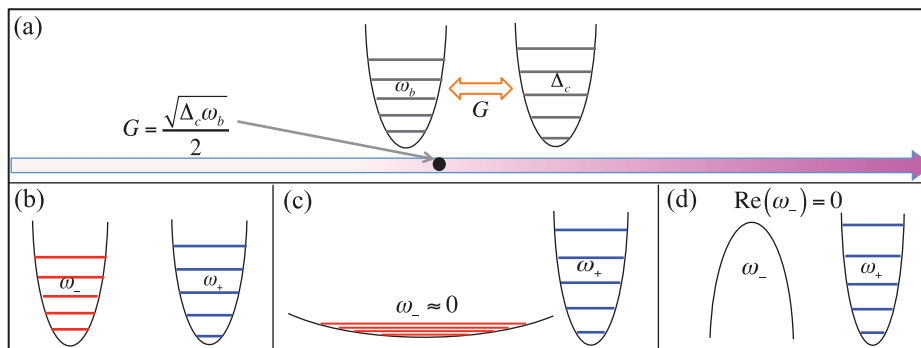


Figure 3 | The critical property of the electromechanical subsystem. (a) The mechanical and electrical modes couple with each other with the coupling strength G . The black circle indicate the quantum critical point. (b,c,d) The effective potential of the normal mode ω_- becomes flat and further inverted when increasing the coupling strength G .

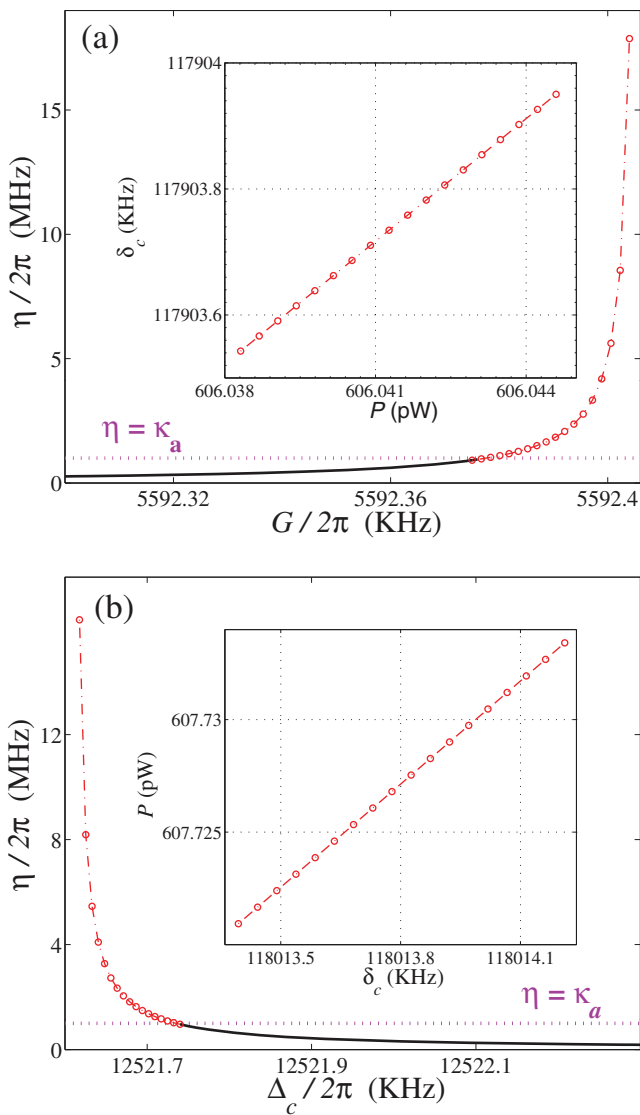


Figure 4 | Controllability of the system parameters. Nonlinear parameter η versus: (a) the coupling strength G and (b) the effective detuning Δ_c . The inserts present the experimental parameter range (the power P and frequency detuning δ_c of the input microwave field) for $\eta > \kappa_a$. The system parameters are the same as those in Fig. 2 except for $\omega_c/2\pi = 7.5$ GHz for the inserts.

The result is

$$\hat{H}_{\text{OMS}}''/\hbar = \tilde{\omega}_a \hat{a}^\dagger \hat{a} - \eta \hat{a}^\dagger \hat{a} \hat{a}^\dagger \hat{a} + \omega_- \hat{B}_-^\dagger \hat{B}_- + \omega_+ \hat{B}_+^\dagger \hat{B}_+, \quad (8)$$

and η is the photon-photon interaction strength,

$$\eta = \frac{g_a^2}{\omega_b - 4G^2/\Delta_c}. \quad (9)$$

Notice that the photon-photon interaction strength η remains unchanged when the system-environment interaction is explicitly included (see the detailed derivation in Methods). On the other hand, it also shows in Figs. 2(c,d) that even in the *weak-coupling regime* $g_m \ll \kappa_m$ ($m=a,c$), a strong photon-photon interaction η ($\eta > \kappa_a$) can still be obtained when G (or Δ_c) approaches the quantum critical point. In particular, Fig. 2 shows that when the coupling strength G (or the detuning Δ_c) is close to its quantum critical point, a very small normal mode frequency ω_- is obtained, which induces a large photon-photon interaction with $\eta \propto 1/\omega_-$. The

system parameters G and Δ_c , determined by the power P and the frequency detuning δ_c of the input microwave driving field, can be directly tuned in experiments. Figure 4 shows explicitly the practical parameter range of P and δ_c for obtaining the strong Kerr nonlinear parameter η ($\eta > \kappa_a$).

Photon blockade. The strong Kerr nonlinearity in the present system can be further demonstrated by the steady-state second-order correlation function of the optical field $g^{(2)}(0)$. $g^{(2)}(0) \rightarrow 0$ in the weak-coupling regime signals the photon blockade effect, and can be directly detected by a Hanbury-Brown-Twiss Interferometer³. Explicitly, by driving the optical cavity with a weak laser field of frequency ω_{ai} and amplitude ε_a , the Hamiltonian of the system becomes

$$\begin{aligned} \hat{H}_{\text{OMS}}^d/\hbar = & \Delta_a \hat{a}^\dagger \hat{a} - \eta \hat{a}^\dagger \hat{a} \hat{a}^\dagger \hat{a} + i\varepsilon_a (\hat{a}^\dagger e^{-\hat{P}} - e^{\hat{P}} \hat{a}) \\ & + \omega_- \hat{B}_-^\dagger \hat{B}_- + \omega_+ \hat{B}_+^\dagger \hat{B}_+, \end{aligned} \quad (10)$$

where all the similarity transformations used before have been taken into account, and $\Delta_a = \tilde{\omega}_a - \omega_{ai}$. The damping effect arising from the coupling of the optical field to the electromagnetic vacuum modes of the environment can also be taken into account, and the dissipative dynamics of cavity mode \hat{a} is described by the quantum Langevin equation,

$$\frac{\partial}{\partial t} \hat{a}(t) = \frac{i}{\hbar} [\hat{H}_{\text{OMS}}^d, \hat{a}(t)] - \kappa_a \hat{a}(t) - \sqrt{2\kappa_a} e^{-\hat{P}} \hat{f}_{\text{in}}(t). \quad (11)$$

Here κ_a is the decay rate of cavity mode \hat{a} and \hat{f}_{in} is a vacuum noise operator satisfying $\langle \hat{f}_{\text{in}} \hat{f}_{\text{in}}^\dagger \rangle = \delta(t-t')$, $\langle \hat{f}_{\text{in}}^\dagger \hat{f}_{\text{in}} \rangle = 0$.

With a weak optical driving field, the quantum Langevin equation is solved by truncating them to the lowest relevant order in ε_a . The resulting two-photon correlation function is given by

$$g^{(2)}(0) = \lim_{t \rightarrow \infty} \frac{\langle \hat{a}^\dagger \hat{a}^\dagger \hat{a} \hat{a} \rangle(t)}{\langle \hat{a}^\dagger \hat{a} \rangle^2(t)} \approx \frac{2P_2(\infty)}{P_1^2(\infty)} \quad (12)$$

with

$$\begin{aligned} \lim_{t \rightarrow \infty} \langle \hat{a}^\dagger \hat{a}^\dagger \hat{a} \hat{a} \rangle(t) = & \frac{2\varepsilon_a^4}{\kappa_a} \text{Re} \int_0^\infty d\tau_1 \int_0^\infty d\tau_2 \\ & \int_0^\infty d\tau_3 e^{(-i\tilde{\Delta}_a + i\eta - \kappa_a)\tau_1} e^{(i\tilde{\Delta}_a - \kappa_a)\tau_2} e^{(-i\tilde{\Delta}_a - \kappa_a)\tau_3} e^{-\Phi_4}, \end{aligned} \quad (13a)$$

$$\lim_{t \rightarrow \infty} \langle \hat{a}^\dagger \hat{a} \rangle(t) = \frac{\varepsilon_a^2}{\kappa_a} \text{Re} \int_0^\infty d\tau \exp \left[-\left(i\tilde{\Delta}_a + \kappa_a \right) \tau \right] \exp(-\Phi_2), \quad (13b)$$

where

$$P_s(t) \simeq \frac{\langle (\hat{a}^\dagger)^s \hat{a}^s \rangle(t)}{s n_0^s}, \quad (s=1,2; n_0 = \varepsilon_a^2 / \kappa_a^2)$$

is the normalized s -photon probability in the cavity ($P_s \gg P_{s+1}$ in the weak-driving regime), and

$$e^{-\Phi_4} = \langle e^{\hat{P}(\tau_1 - \tau_2)} e^{\hat{P}(\tau_1)} e^{-\hat{P}(0)} e^{-\hat{P}(-\tau_3)} \rangle,$$

$$e^{-\Phi_2} = \langle e^{\hat{P}(\tau)} e^{-\hat{P}(0)} \rangle, \quad \tilde{\Delta}_a = \Delta_a - \eta.$$

Note that $\hat{P} = \zeta_- \hat{P}_- - \zeta_+ \hat{P}_+$ is a complex operator including the microwave field \hat{c} and the mechanical mode \hat{b} , and $\hat{P}_j(t)$ ($j=\pm$) is determined by the dynamics of the electromechanical modes B_j , which evolves as

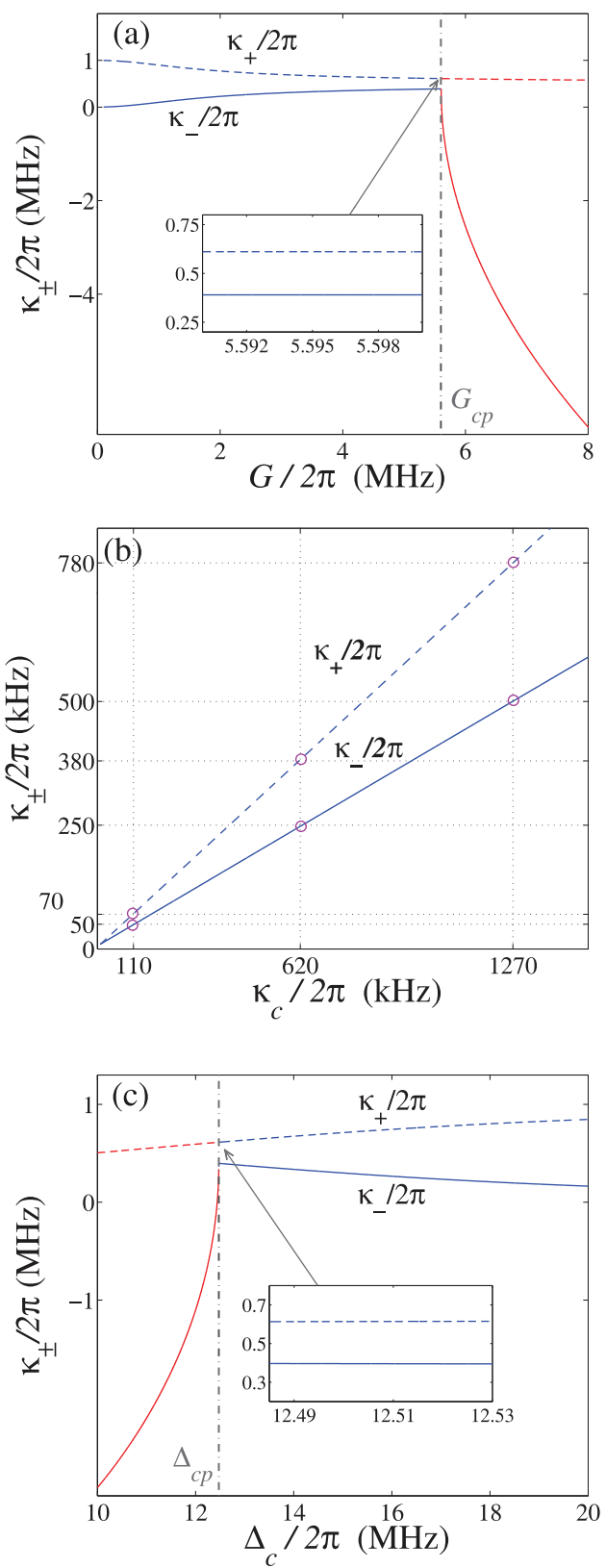


Figure 5 | Effective decay rates for the electromechanical normal modes. Effective decay rates κ_{\pm} of the normal modes ω_{\pm} versus: (a) the coupling strength G , (b) the decay rate of microwave field κ_c , and (c) the detuning Δ_c . The system parameters are $\Delta_c/2\pi = 12.51$ MHz, $\kappa_d/2\pi = 1$ MHz for (a), while $G/2\pi = 5.5924$ MHz, $\Delta_c/2\pi = 12.51$ MHz for (b), and $G/2\pi = 5.595$ MHz, $\kappa_d/2\pi = 1$ MHz for (c). The purple circles in (b) indicate the parameter regime corresponding to the κ_{\pm} used in Fig. 6.

$$\frac{\partial}{\partial t} \hat{B}_- = (-i\omega_- - \kappa_-) \hat{B}_- - \sqrt{2\kappa_-} \hat{l}_{in}, \quad (14a)$$

$$\frac{\partial}{\partial t} \hat{B}_+ = (-i\omega_- - \kappa_+) \hat{B}_+ - \sqrt{2\kappa_+} \hat{l}_{in}. \quad (14b)$$

The noise operator $\hat{l}_{in}(t) = \frac{1}{\sqrt{2\pi}} \int d\omega \hat{l}_0(\omega) e^{-i(\omega - \omega_{ci})t}$, which comes from the environment of the microwave resonator. The environment is initially in the thermal equilibrium state ρ_{th} with temperature T , and $\hat{l}_0(\omega)$ is the initial environment operators of the microwave resonator. Here, we have safely ignored the dissipation of the mechanical oscillator because the mechanical decay rate κ_b is extremely small, $\kappa_b/\kappa_a, \kappa_b/\kappa_c < 10^{-3}$. Thus, the effective decay rates κ_j is determined by the original decay rate of the microwave resonator κ_c (see the detailed derivation in Methods).

In Fig. 5, we show the dependences of κ_{\pm} on the system parameters G , Δ_c and κ_c . From Fig. 5 one can see that the effective decay rate κ_- sharply changes from a positive value to a negative value when the system parameter G (or Δ_c) crosses its quantum critical point G_{cp} (or Δ_{cp}). This result demonstrates that the mode ω_- will become a gain mode when $G > G_{cp}$ or $\Delta_c < \Delta_{cp}$. Near the quantum critical points G_{cp} and Δ_{cp} , the effective decays κ_{\pm} almost become constant with G or Δ_c [see the inserts of Fig. 5(a) and 5(c)]. In Fig. 5(b) κ_{\pm} is plotted via the microwave field decay rate κ_c when G (or Δ_c) is near the quantum critical points. As it is shown, κ_{\pm} exhibit a linear increase with the decay rate of the microwave field κ_c .

When the microwave (mechanical) mode is initially in the coherent state $|\alpha\rangle$ ($|\beta\rangle$), and the optical field in the vacuum state, the two-point correlation function $\exp(-\Phi_2)$ and the four-point correlation function $\exp(-\Phi_4)$ are calculated. With numerically integrating Eqs. (13), the dependence of $g^{(2)}(0)$ on κ_- , G , and Δ_c is shown in Fig. 6. As one see, in the quantum critical regime, the photon antibunching effect $g^{(2)}(0) < 1$ (even the photon blockade $g^{(2)}(0) \rightarrow 0$) occurs because the two-photon transition is largely suppressed in comparison with the single-photon transition when $\kappa_-/2\pi > 60$ kHz [see the insert in Fig. 6(a)]. Figures 6(b) and (c) further show that the photon blockade [$g^{(2)}(0) \rightarrow 0$] occurs when the tunable parameter G (or Δ_c) approaches its quantum critical value even if the optomechanical coupling g_a is very weak.

Furthermore, we also find that the photon antibunching [$g^{(2)}(0) < 1$] disappears when $\kappa_-/2\pi < 60$ kHz [see the inserts in Figs. 6(b) and (c)]. Physically, this is because in the hybrid OMS, a relatively large decay rate κ_- ($\kappa_-/2\pi > 60$ kHz) occurs when the electromechanical subsystem approaches the quantum critical point. This decay will significantly suppress the steady-state sideband transition in the electromechanical subsystem. Then, in the quantum critical regime, the hybrid OMS becomes a pure optical nonlinear system, and $\eta > \kappa_a$ is the exclusive condition for achieving the photon blockade. Meanwhile, the very small ω_- ($\omega_- \rightarrow 10$ kHz) near the quantum critical point effectively enhances the photon-photon interaction to $\eta > \kappa_a$ because $\eta \propto 1/\omega_-$, namely the photon blockade can still be reachable even if the effective electromechanical frequency extends beyond the resolved sideband regime, i.e. $\omega_- < \kappa_a$. Notice that the original mechanical frequency used here is still in the resolved sideband regime ($\omega_b \gg \kappa_a$) so that there is no problem in cooling the mechanical oscillator at the initial time.

Nonclassical states. As demonstrated in previous studies^{21–23}, strong Kerr nonlinearities generally lead to the periodic generation of nonclassical states, (e.g., cat states) of the cavity field. With the help of the Hamiltonian (4), we obtain the time evolution operator in the interaction picture,

$$\begin{aligned} \hat{U}(t) \approx & \exp(i\eta \hat{a}^\dagger \hat{a} \hat{a}^\dagger \hat{a}^\dagger) \\ & \exp\left\{\zeta \hat{a}^\dagger \hat{a} [\hat{B}_+^\dagger (1 - e^{-i\omega_- t}) - \hat{B}_- (1 - e^{i\omega_- t})]\right\}, \end{aligned} \quad (15)$$

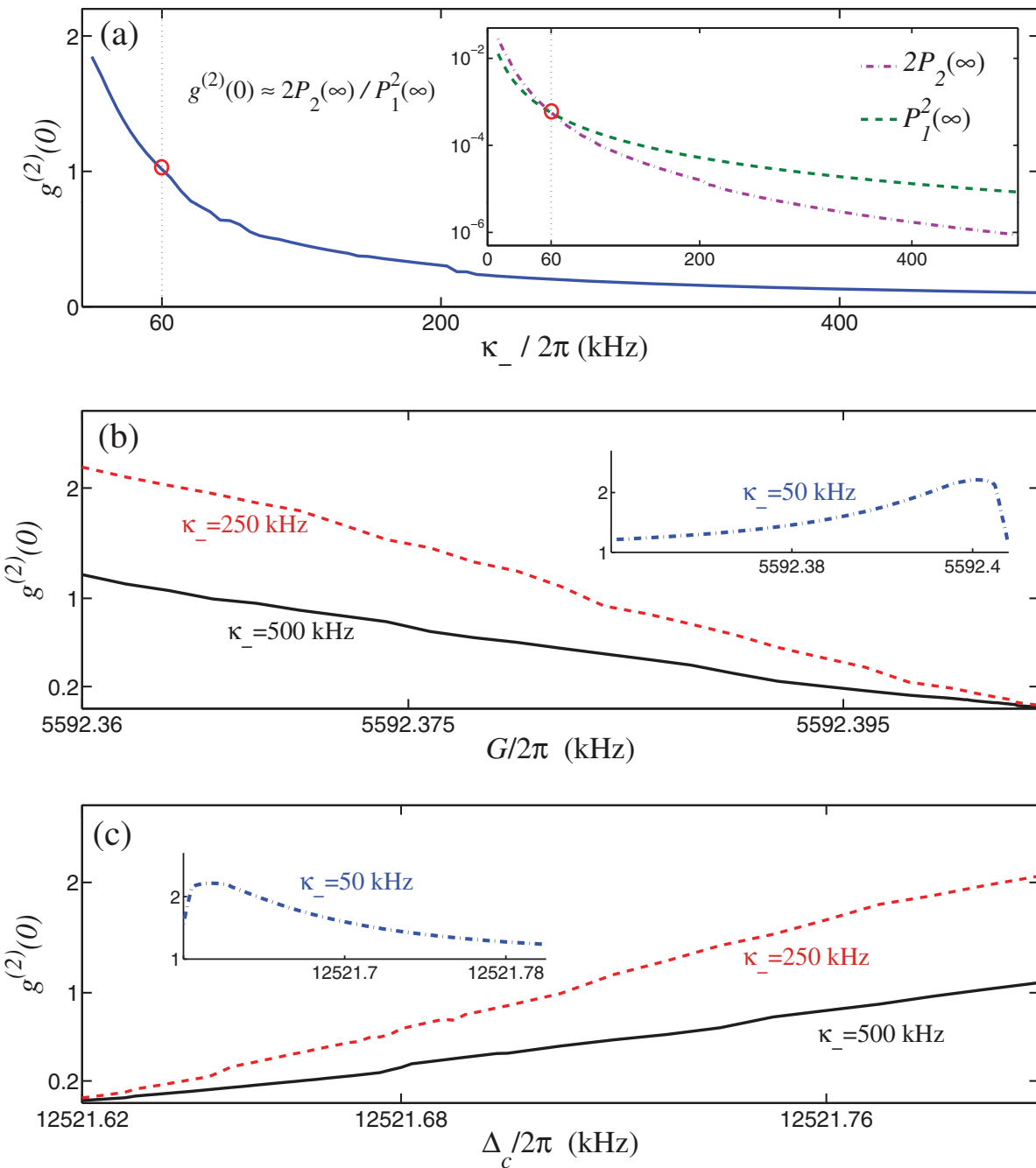


Figure 6 | Photon statistics in the hybrid electro-optomechanical system. Equal-time second-order correlation function $g_s^{(2)}(0)$ versus: (a) effective decay rate κ_- , (b) coupling strength G , and (c) detuning Δ_c at $T = 0$ for the microwave bath. The red circles in (a) indicate the value of κ_- for $g_s^{(2)}(0) = 1$. We have chosen the quantum critical parameters: $G/2\pi = 5595$ kHz, $\Delta_c/2\pi = 12521.64$ kHz in (a), and the decay rates $\kappa_-/2\pi = (500, 250, 50)$ kHz (corresponding to $\kappa_c/2\pi = (1270, 620, 110)$ kHz) in (b,c). The other parameters are the same as in Fig. 2, except for $\Delta_a = \eta$ in order to maximize the photon antibunching effect.

where the term corresponding to ζ_+ has been omitted due to its negligible effect on the evolution of the cavity mode \hat{a} ($\zeta_+/\omega_b \sim 10^{-4}$) near the quantum critical point. If the cavity field \hat{a} is initially in a coherent state $|\Upsilon\rangle$, the cavity field at time $t_n = 2n\pi/\omega_-$ ($n = 1, 2, \dots$) will be in the state

$$|\Psi_a(t_n)\rangle = \exp(-|\Upsilon|^2/2) \sum_{m=0}^{\infty} \frac{\Upsilon^m}{\sqrt{m!}} \exp\left(i \frac{2n\pi\eta}{\omega_-} m^2\right) |m\rangle_a. \quad (16)$$

The state $|\Psi_a(t_n)\rangle$ is a multi-component cat state, depending on the value of η/ω_- . Figure 7 shows the different multi-component cat

states for different values of the tunable parameters G and Δ_c near the quantum critical point. Figures 7(b,c,d) present the specific realization of two-, three- and four-component cat states, respectively. Here damping effects (given by $\kappa_a, \kappa_c, \kappa_b$) have been ignored. In principle, this is valid when the cut-off time $t_n \ll 1/\kappa_a, 1/\kappa_c, 1/\kappa_b$. The optical field damping is similar to that in a recent cavity-QED experiment⁵⁴. Moreover, inspired by Ref. 54, the Wigner function can be measured (or reconstructed) by detecting the states of the atoms interacting with the optical field. Nevertheless, the above result indicates that the quantum-criticality-induced strong Kerr nonlinearities in this hybrid OMS can generate

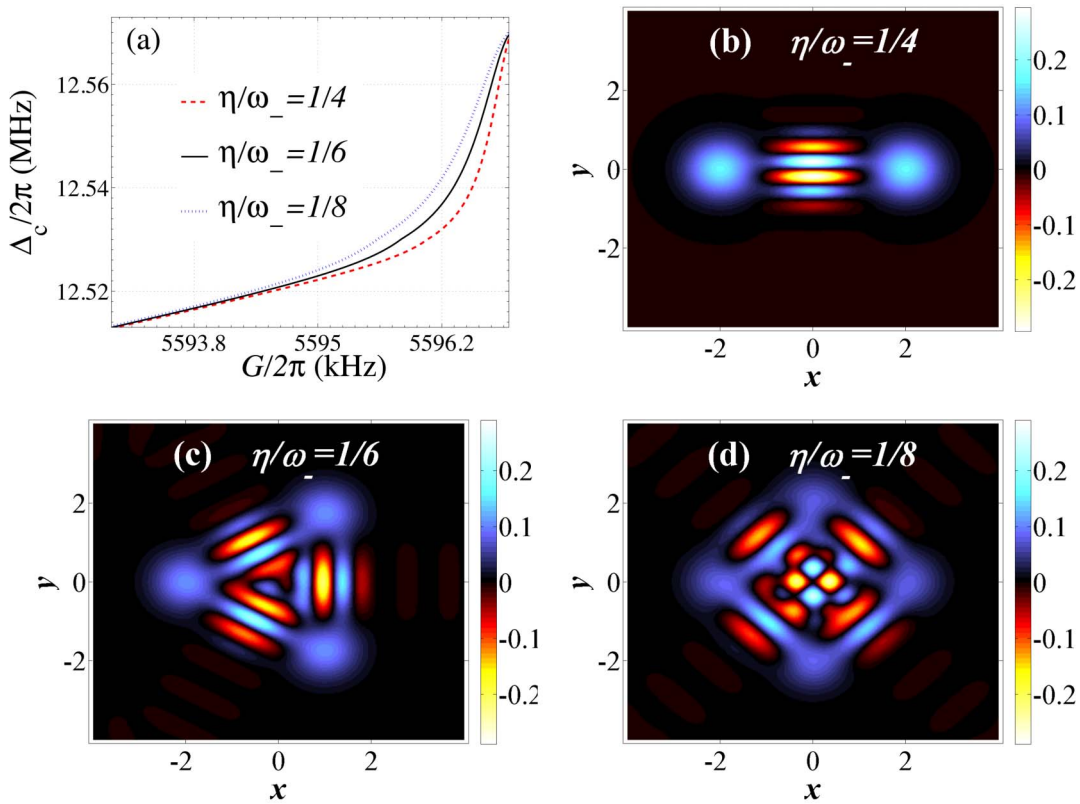


Figure 7 | Parameter regimes (a) for obtaining the two- (b), three- (c) and four-component (d) Schrödinger cat state. The quadratures variables are $x = (\hat{a} + \hat{a}^\dagger)/\sqrt{2}$, $y = -i(\hat{a} - \hat{a}^\dagger)/\sqrt{2}$. The system parameters are the same as in Fig. 2 except for $\Upsilon = 2$.

nonclassical states by cutting off the optomechanical interaction at the appropriate time, which can be detected via Wigner tomography.

Discussion

We have provided a new mechanism for obtaining strong Kerr nonlinear effects in a hybrid OMS in the *weak-coupling regime*. We found that the electromechanical subsystem displays a critical property when adjusting the intensity (or frequency) of the microwave driving field, and a strong controllable photon-photon interaction is induced in the quantum critical regime. Usually, the phonon modulation effect influences the photon statistics in the usual OMSs²⁴, and in general will also weaken the photon-photon interaction effect, except in the single-photon strong-coupling ($g_a > \kappa_a$) and the resolved sideband ($\kappa_a \ll \omega_b$) regime²⁴. The essence of the strong photon-photon interaction presented in this paper can be understood as follows. In the quantum critical regime, the electromechanical normal mode \hat{B}_- coupled to the optical field is highly softened (or a very small normal-mode frequency ω_- is obtained). At the same time, the sideband phonon transitions in the electromechanical subsystem are significantly suppressed by the relative large decay rate of the electromechanical normal mode, which makes the hybrid OMS essentially a pure optical nonlinear system. Thus, the quantum-criticality-induced strong self-Kerr nonlinearity is very different from previous investigations in the usual OMSs^{24,34,35}.

Experimentally, the strong photon-photon interaction achieved in the present hybrid OMS requires driving the electromechanical subsystem into its quantum critical region (shaded area in Fig. 2). Normal-mode splitting in the driven electromechanical system has been observed⁴³. The quantum critical region could be easily reached by increasing the intensity of the microwave driving field. Moreover, as shown in Figs. 2 and 4, the interesting ranges of G and Δ_c are respectively on the order of 0.1 kHz and 1 kHz for the quantum critical region, and this parameter precision is experimentally

realizable⁵⁵. We believe that our proposal will provide a new avenue for experimentally realizing strong optical nonlinearities in the *weak-coupling regime* and largely enrich the scope of implementing quantum information processing and quantum metrology with cavity OMSs.

Methods

Derivation of the photon-photon interaction with system-environment couplings. The total Hamiltonian of the hybrid OMS plus the environment can be written as

$$\hat{H}_{\text{tot}} = \hat{H}'_{\text{OMS}} + \hat{H}_{\text{E}} + \hat{H}_{\text{SE}} \quad (17a)$$

where the system Hamiltonian \hat{H}'_{OMS} is given by Eq. (4) and

$$\begin{aligned} \hat{H}_{\text{E}}/\hbar = & \int d\omega \hat{f}^\dagger(\omega) \hat{f}(\omega) + \int d\omega \hat{h}^\dagger(\omega) \hat{h}(\omega) \\ & + \int d\omega (\omega - \omega_a) \hat{l}^\dagger(\omega) \hat{l}(\omega), \end{aligned} \quad (17b)$$

$$\begin{aligned} \hat{H}_{\text{SE}}/\hbar = & i \int d\omega K_a(\omega) [\hat{a}^\dagger \hat{f}(\omega) - \hat{f}^\dagger(\omega) \hat{a}] + i \int d\omega K_c(\omega) [\hat{c}^\dagger \hat{l}(\omega) - \hat{l}^\dagger(\omega) \hat{c}] \\ & + \int d\omega K_b(\omega) [\hat{b}^\dagger \hat{h}(\omega) + \hat{h}^\dagger(\omega) \hat{b}], \end{aligned} \quad (17c)$$

are the Hamiltonians of the environment and the system-environment interaction, respectively. Notice that the system-environment interaction is invariant to the linearization procedure applied on the electromechanical subsystem. Here $\hat{f}(\omega)$, $\hat{h}(\omega)$, $\hat{l}(\omega)$ are the bath operators for \hat{a} , \hat{b} , \hat{c} , and $K_j(\omega)$ ($j = a, b, c$) are the corresponding coupling constants. For a slowly-varying bath spectrum, we can simply replace $K_j(\omega)$ by the decay rate $\sqrt{\kappa_j}/\pi$. Here the last term can be safely neglected because the decay rate κ_b of the mechanical oscillator is extremely small ($\kappa_b/\kappa_a, \kappa_b/\kappa_c < 10^{-3}$).

By applying a Bogoliubov transformation $\hat{R} = M\hat{B}$ to the total Hamiltonian \hat{H}_{tot} , the hybrid OMS Hamiltonian \hat{H}'_{OMS} and the interaction between the system and the environment \hat{H}_{SE} can be rewritten in terms of the normal-mode canonical operators



$$\hat{H}'_{\text{OMS}}/\hbar = \omega_- \hat{B}_-^\dagger \hat{B}_- + \omega_+ \hat{B}_+^\dagger \hat{B}_+ + \tilde{\omega}_a \hat{a}^\dagger \hat{a} - g_- \hat{a}^\dagger \hat{a} (\hat{B}_-^\dagger + \hat{B}_-) + g_+ \hat{a}^\dagger \hat{a} (\hat{B}_+^\dagger + \hat{B}_+), \quad (18a)$$

$$\begin{aligned} \hat{H}_{\text{SE}}/\hbar &= i \sqrt{\frac{\kappa_a}{\pi}} \int d\omega [\hat{a}^\dagger \hat{f}(\omega) - \hat{f}^\dagger(\omega) \hat{a}] \\ &+ i \sqrt{\frac{\kappa_c}{\pi}} \int d\omega \left[(M_{12} \hat{B}_- + M_{11} \hat{B}_-^\dagger + M_{14} \hat{B}_+ + M_{13} \hat{B}_+^\dagger) \hat{l}(\omega) \right. \\ &\left. - \hat{l}^\dagger(\omega) (M_{11} \hat{B}_- + M_{12} \hat{B}_-^\dagger + M_{13} \hat{B}_+ + M_{14} \hat{B}_+^\dagger) \right], \end{aligned} \quad (18b)$$

while the environment Hamiltonian \hat{H}_{E} retains its original form.

To derive the photon-photon interaction, the total Hamiltonian should be further diagonalized in a displaced-oscillator representation, $\hat{H}'_{\text{tot}} = \hat{V}^\dagger \hat{H}_{\text{tot}} \hat{V}$, and the result is

$$\hat{H}_{\text{OMS}}''/\hbar = \tilde{\omega}_a \hat{a}^\dagger \hat{a} - \eta \hat{a}^\dagger \hat{a} \hat{a}^\dagger \hat{a} + \omega_- \hat{B}_-^\dagger \hat{B}_- + \omega_+ \hat{B}_+^\dagger \hat{B}_+, \quad (19a)$$

$$\begin{aligned} \hat{H}_{\text{SE}}'/\hbar &= i \sqrt{\frac{\kappa_a}{\pi}} \int d\omega [\hat{a}^\dagger e^{-P} \hat{f}(\omega) - \hat{f}^\dagger(\omega) e^P \hat{a}] \\ &+ i \sqrt{\frac{\kappa_c}{\pi}} \int d\omega \left[(M_{12} \hat{B}_- + M_{11} \hat{B}_-^\dagger + M_{14} \hat{B}_+ + M_{13} \hat{B}_+^\dagger) \hat{l}(\omega) \right. \\ &\left. - \hat{l}^\dagger(\omega) (M_{11} \hat{B}_- + M_{12} \hat{B}_-^\dagger + M_{13} \hat{B}_+ + M_{14} \hat{B}_+^\dagger) \right] \\ &- i \sqrt{\frac{\kappa_c}{\pi}} [(M_{11} + M_{12}) \zeta_- + (M_{13} + M_{14}) \zeta_+] \hat{a}^\dagger \hat{a} \int d\omega [\hat{l}(\omega) - \hat{l}^\dagger(\omega)], \end{aligned} \quad (19b)$$

where

$$\eta = \frac{g_a^2}{\omega_b - 4G^2/\Delta_c} \quad (20)$$

is the photon-photon interaction strength. This similarity transformation also does not affect the environment Hamiltonian \hat{H}_{E} . By comparing with the dissipation Hamiltonian in the original representation [Eq. (18b)], it can be seen that the last term of Eq. (19b) is induced by the similarity transformation in the displaced-oscillator representation, and it may change the photon-photon interaction. However, we will show next that, in the quantum critical regime, this term will not change the photon-photon interaction η , and it only induces a negligible pure-dephase of the optical mode.

In the quantum critical regime, the system parameters M_{13} , M_{14} , and ζ_+ are negligible compared to the parameters M_{11} , M_{12} , and ζ_- , due to the relative large frequency ω_+ (M_{13} , M_{14} , and ζ_+ are smaller than M_{11} , M_{12} , and ζ_- by about 3 to 4 orders of magnitude). This means that the influence of the normal mode B_+ on the dynamics of the optical mode \hat{a} can be safely neglected when the electromechanical subsystem approaches its quantum critical point. By ignoring the normal modes \hat{B}_+ , the dynamics of the bath operator $\hat{l}(\omega)$ can be determined by the following equation of motion,

$$\frac{d\hat{l}(\omega)}{dt} = -i(\omega - \omega_{ci})\hat{l}(\omega) = \sqrt{\frac{\kappa_c}{\pi}} [M_{11} \hat{B}_- + M_{12} \hat{B}_-^\dagger - (M_{11} + M_{12}) \zeta_- \hat{a}^\dagger \hat{a}]. \quad (21)$$

Solving Eq. (21), the result is

$$\begin{aligned} \hat{l}(\omega) &= e^{-i(\omega - \omega_{ci})t} \hat{l}_0(\omega) + \sqrt{\frac{\kappa_c}{\pi}} \int_0^t ds e^{-i(\omega - \omega_{ci})(t-s)} \\ &\left. \left\{ \zeta_- (M_{11} + M_{12}) \hat{a}^\dagger \hat{a}(s) - [M_{11} \hat{B}_-(s) + M_{12} \hat{B}_-^\dagger(s)] \right\} \right\}, \end{aligned} \quad (22)$$

where $\hat{l}_0(\omega)$ is the initial environment operator of the microwave resonator. Substituting the above solution of the bath operator and its hermitian conjugate into the last term of Eq. (19b) and noticing that in the quantum-critical-regime $M_{11} \simeq M_{12}$, we have

$$\begin{aligned} i \sqrt{\frac{\kappa_c}{\pi}} (M_{11} + M_{12}) \zeta_- \hat{a}^\dagger \hat{a} \int d\omega [\hat{l}(\omega) - \hat{l}^\dagger(\omega)] &= \\ -i \sqrt{2\kappa_c} (M_{11} + M_{12}) \zeta_- \hat{a}^\dagger \hat{a} [\hat{l}_{in}(t) - \hat{l}_{in}^\dagger(t)]. \end{aligned} \quad (23)$$

Therefore, the photon-photon interaction given in Eq. (19a) remains invariant under the interaction with the environment.

Calculation of the effective decay rates for the electromechanical normal modes. Based on the dissipative dynamics of the electro-mechanical subsystem in the original representation, we can find the relationship between the effective decay rates κ_\pm and the original decay rates of the microwave resonator κ_c .

Considering the thermal environments of the microwave resonator, the Hamiltonian of the electro-mechanical subsystem plus the environment is

$$\begin{aligned} \hat{H}_{\text{sub}} &= \Delta_c \hat{c}^\dagger \hat{c} + \omega_b \hat{b}^\dagger \hat{b} - G(\hat{c}^\dagger + \hat{c})(\hat{b}^\dagger + \hat{b}) \\ &+ i \sqrt{\frac{\kappa_c}{\pi}} \int d\omega [\hat{c}^\dagger \hat{l}(\omega) - \hat{l}^\dagger(\omega) \hat{c}], \end{aligned} \quad (24)$$

Then, the dynamics of the canonical operator \hat{R} is given by

$$\begin{aligned} \frac{\partial}{\partial t} \hat{R}(t) &= -i[\hat{R}(t), \hat{H}_{\text{opt}}] - \Gamma \hat{R}(t) - \sqrt{2\Gamma} \hat{F}_{\text{in}}(t) \\ &= D \hat{R}(t) - \sqrt{2\Gamma} \hat{F}_{\text{in}}(t), \end{aligned} \quad (25)$$

where the coefficient matrix

$$D = \begin{pmatrix} -i\Delta_c - \kappa_c & 0 & iG & iG \\ 0 & i\Delta_c - \kappa_c & -iG & -iG \\ iG & iG & -i\omega_b & 0 \\ -iG & -iG & 0 & i\omega_b \end{pmatrix}.$$

Here, $\Gamma = \text{diag}(\kappa_c, \kappa_c, 0, 0)$ denotes the decay rates of the microwave resonator and the mechanical oscillator, and $\hat{F}_{\text{in}}^T(t) = (\hat{l}_{in}, \hat{l}_{in}^\dagger, \hat{h}_{in}, \hat{h}_{in}^\dagger)$ are the Langevin forces. Equation (25) shows that the imaginary and real parts of the eigenvalues of D correspond to the eigenfrequencies ω_\pm and the effective decay rates κ_\pm of the normal modes. For the undamped case ($\kappa_c = 0$), the eigenvalues of D are purely imaginary and we obtain the expression Eq. (5) for the normal-mode frequencies. For the general κ_c , we numerically diagonalized the coefficient matrix D and shown the results in Fig. 5.

1. Imamoğlu, A., Schmidt, H., Woods, G. & Deutsch, M. Strongly Interacting Photons in a Nonlinear Cavity. *Phys. Rev. Lett.* **79**, 1467–1470 (1997).
2. Werner, M. J. & Imamoğlu, A. Photon-photon interactions in cavity electromagnetically induced transparency. *Phys. Rev. A* **61**, 011801(R) (1999).
3. Birnbaum, K. M. *et al.* Photon blockade in an optical cavity with one trapped atom. *Nature* **436**, 87–90 (2005).
4. Ourjoumtsev, A. *et al.* Observation of squeezed light from one atom excited with two photons. *Nature* **474**, 623–626 (2011).
5. Brune, M. *et al.* Manipulation of photons in a cavity by dispersive atom-field coupling: Quantum-nondemolition measurements and generation of “Schrödinger cat” states. *Phys. Rev. A* **45**, 5193–5214 (1992).
6. Xiao, Y.-F. *et al.* Quantum nondemolition measurement of photon number via optical Kerr effect in an ultra-high-Q microtoroid cavity. *Optics Express* **16**, 21462–21475 (2008).
7. Dayan, B. *et al.* A Photon Turnstile Dynamically Regulated by One Atom. *Science* **319**, 1062–1065 (2008).
8. Miranowicz, A., Tanaś, R. & Kielich, S. Generation of discrete superpositions of coherent states in the anharmonic oscillator model. *Quantum Opt.* **2**, 253–265 (1990).
9. Wu, Y. & Deng, L. Ultraslow Optical Solitons in a Cold Four-State Medium. *Phys. Rev. Lett.* **93**, 143904 (2004).
10. Hartmann, M. J., Brandão, F. G. S. L. & Plenio, M. B. Strongly interacting polaritons in coupled arrays of cavities. *Nature Physics* **2**, 849–855 (2006).
11. Rebić, S., Twamley, J. & Milburn, G. J. Giant Kerr Nonlinearities in Circuit Quantum Electrodynamics. *Phys. Rev. Lett.* **103**, 150503 (2009).
12. Liu, Y. X. *et al.* Qubit-induced phonon blockade as a signature of quantum behavior in nanomechanical resonators. *Phys. Rev. A* **82**, 032101 (2010).
13. You, J. Q. & Nori, F. Superconducting circuits and quantum information. *Physics Today* **58**(11), 42–47 (2005).
14. You, J. Q. & Nori, F. Atomic physics and quantum optics using superconducting circuits. *Nature* **474**, 589–597 (2011).
15. Buluta, I., Ashhab, S. & Nori, F. Natural and artificial atoms for quantum computation. *Rep. Prog. Phys.* **74**, 104401 (2011).
16. Jacobs, K. & Landahl, A. J. Engineering Giant Nonlinearities in Quantum Nanosystems. *Phys. Rev. Lett.* **103**, 067201 (2009).
17. Zhang, J., Wu, R.-B., Liu, Y. X., Li, C.-W. & Tarn, T.-J. Quantum Coherent Nonlinear Feedback With Applications to Quantum Optics on Chip. *IEEE Trans. Automat. Contr.* **57**, 1997–2008 (2012).
18. Aspelmeyer, M., Meystre, P. & Schwab, K. Quantum optomechanics. *Physics Today* **65**(7), 29–35 (2012).
19. Kippenberg, T. J. & Vahala, K. J. Cavity Optomechanics: Back-Action at the Mesoscale. *Science* **321**, 1172–1176 (2008).
20. Marquardt, F. & Girvin, S. M. Trend: Optomechanics. *Physics* **2**, 40 (2009).
21. Mancini, S., Man’ko, V. I. & Tombesi, P. Ponderomotive control of quantum macroscopic coherence. *Phys. Rev. A* **55**, 3042–3050 (1997).
22. Bose, S., Jacobs, K. & Knight, P. L. Preparation of nonclassical states in cavities with a moving mirror. *Phys. Rev. A* **56**, 4175–4186 (1997).
23. Marshall, W., Simon, C., Penrose, R. & Bouwmeester, D. Towards Quantum Superpositions of a Mirror. *Phys. Rev. Lett.* **91**, 130401 (2003).
24. Rabl, P. Photon Blockade Effect in Optomechanical Systems. *Phys. Rev. Lett.* **107**, 063601 (2011).



25. Nunnenkamp, A., Børkje, K. & Girvin, S. M. Single-Photon Optomechanics. *Phys. Rev. Lett.* **107**, 063602 (2011).
26. Gong, Z. R., Ian, H., Liu, Y. X., Sun, C. P. & Nori, F. Effective Hamiltonian approach to the Kerr nonlinearity in an optomechanical system. *Phys. Rev. A* **80**, 065801 (2009).
27. He, B. Quantum optomechanics beyond linearization. *Phys. Rev. A* **85**, 063820 (2012).
28. Xu, X. W., Li, Y. J. & Liu, Y. X. Photon-induced tunneling in optomechanical systems. *Phys. Rev. A* **87**, 025803 (2013).
29. Kronwald, A., Ludwig, M. & Marquardt, F. Full photon statistics of a light beam transmitted through an optomechanical system. *Phys. Rev. A* **87**, 013847 (2013).
30. Liao, J.-Q., Cheung, H. K. & Law, C. K. Spectrum of single-photon emission and scattering in cavity optomechanics. *Phys. Rev. A* **85**, 025803 (2012).
31. Liao, J.-Q. & Law, C. K. Correlated two-photon scattering in cavity optomechanics. *Phys. Rev. A* **87**, 043809 (2013).
32. Xiong, H., Si, L.-G., Zheng, A.-S., Yang, X. & Wu, Y. Higher-order sidebands in optomechanically induced transparency. *Phys. Rev. A* **86**, 013815 (2012).
33. Zhang, K., Meystre, P. & Zhang, W. Role Reversal in a Bose-Condensed Optomechanical System. *Phys. Rev. Lett.* **108**, 240405 (2012).
34. Stannigel, K. *et al.* Optomechanical Quantum Information Processing with Photons and Phonons. *Phys. Rev. Lett.* **109**, 013603 (2012).
35. Ludwig, M., Safavi-Naeini, A. H., Painter, O. & Marquardt, F. Enhanced Quantum Nonlinearities in a Two-Mode Optomechanical System. *Phys. Rev. Lett.* **109**, 063601 (2012).
36. Gröblacher, S. *et al.* Demonstration of an ultracold micro-optomechanical oscillator in a cryogenic cavity. *Nature Physics* **5**, 485–488 (2009).
37. Rocheleau, T. *et al.* Preparation and detection of a mechanical resonator near the ground state of motion. *Nature* **463**, 72–75 (2010).
38. Verhagen, E., Deleglise, S., Weis, S., Schliesser, A. & Kippenberg, T. J. Quantum-coherent coupling of a mechanical oscillator to an optical cavity mode. *Nature* **482**, 63–67 (2012).
39. Brennecke, F., Ritter, S., Donner, T. & Esslinger, T. Cavity Optomechanics with a Bose-Einstein Condensate. *Science* **322**, 235–238 (2008).
40. Eichenfield, M., Chan, J., Camacho, R. M., Vahala, K. J. & Painter, O. Optomechanical crystals. *Nature* **462**, 78–82 (2009).
41. Gröblacher, S., Hammerer, K., Vanner, M. R. & Aspelmeyer, M. Observation of strong coupling between a micromechanical resonator and an optical cavity field. *Nature* **460**, 724–727 (2009).
42. Teufel, J. D. *et al.* Circuit cavity electromechanics in the strong coupling regime. *Nature* **471**, 204–208 (2011).
43. Akram, U., Kiesel, N., Aspelmeyer, M. & Milburn, G. J. Single-photon optomechanics in the strong coupling regime. *New J. Phys.* **12**, 083030 (2010).
44. Regal, C. A. & Lehnert, K. W. From cavity electromechanics to cavity optomechanics. *J. Phys. Conf. Ser.* **264**, 012025 (2011).
45. Wang, Y.-D. & Clerk, A. A. Using Interference for High Fidelity Quantum State Transfer in Optomechanics. *Phys. Rev. Lett.* **108**, 153603 (2012).
46. Tian, L. Adiabatic State Conversion and Pulse Transmission in Optomechanical Systems. *Phys. Rev. Lett.* **108**, 153604 (2012).
47. Barzanjeh, Sh., Abdi, M., Milburn, G. J., Tombesi, P. & Vitali, D. Reversible Optical-to-Microwave Quantum Interface. *Phys. Rev. Lett.* **109**, 130503 (2012).
48. Law, C. K. Interaction between a moving mirror and radiation pressure: A Hamiltonian formulation. *Phys. Rev. A* **51**, 2537–2541 (1995).
49. Pace, A. F., Collett, M. J. & Walls, D. F. Quantum limits in interferometric detection of gravitational radiation. *Phys. Rev. A* **47**, 3173–3189 (1993).
50. Vitali, D. *et al.* M. Optomechanical Entanglement between a Movable Mirror and a Cavity Field. *Phys. Rev. Lett.* **98**, 030405 (2007).
51. Wilson-Rae, I., Nooshi, N., Zwerger, W. & Kippenberg, T. J. Theory of Ground State Cooling of a Mechanical Oscillator Using Dynamical Backaction. *Phys. Rev. Lett.* **99**, 093901 (2007).
52. Marquardt, F., Chen, J. P., Clerk, A. A. & Girvin, S. M. Quantum Theory of Cavity-Assisted Sideband Cooling of Mechanical Motion. *Phys. Rev. Lett.* **99**, 093902 (2007).
53. Sudhir, V., Genoni, M. G., Lee, J. & Kim, M. S. Critical behavior in ultrastrongly coupled oscillators. *Phys. Rev. A* **86**, 012316 (2012).
54. Deléglise, S. *et al.* Reconstruction of non-classical cavity field states with snapshots of their decoherence. *Nature* **455**, 510–514 (2008).
55. Fortier, T. M. *et al.* Generation of ultrastable microwaves via optical frequency division. *Nature Photonics* **5**, 425–429 (2011).

Acknowledgements

X.Y.L. thanks J. Liu, J. Zhang, J.-Q. Liao, G.-R. Jin, and K. Jacobs for valuable discussions. F.N. and S.A. were partially supported by the ARO, RIKEN iTHESS program, MURI Center for Dynamic Magneto-Optics, JSPS-RFBR Contract No. 12-02-92100, Grant-in-Aid for Scientific Research (S), MEXT Kakenhi on Quantum Cybernetics, and the JSPS via its FIRST program. Y.W. was partially supported by the National Science Foundation (NSF) of China (Grants No. 10975054 and No. 11375067), the National Fundamental Research Program of China (Grant No. 2012CB922103). W.M.Z. was supported by the National Science Council of ROC under Contract No. NSC-99-2112-M-006-008-MY3, and the National Center for Theoretical Science of Taiwan. X.Y.L. was supported by Japanese Society for the Promotion of Science (JSPS) Foreign Postdoctoral Fellowship No. P12204 and the NSF of China under grant numbers 11005057 and 11374116.

Author contributions

X.Y.L. carried out all calculations under the guidance of W.M.Z. and S.A., Y.W. and F.N. participated in the discussions. All authors contributed to the interpretation of the work and the writing of the manuscript.

Additional information

Competing financial interests: The authors declare no competing financial interests.

How to cite this article: Lü, X., Zhang, W., Ashhab, S., Wu, Y. & Nori, F. Quantum-criticality-induced strong Kerr nonlinearities in optomechanical systems. *Sci. Rep.* **3**, 2943; DOI:10.1038/srep02943 (2013).

This work is licensed under a Creative Commons Attribution 3.0 Unported license. To view a copy of this license, visit <http://creativecommons.org/licenses/by/3.0/>